Available online at www.sciencedirect.com

ScienceDirect

Geochimica et Cosmochimica Acta 75 (2011) 2924–2939

Geochimica et Cosmochimica Acta

www.elsevier.com/locate/gca

Experimental investigation of the solubility of albite and jadeite in H_2O, with paragonite + quartz at 500 and 600 °C, and 1–2.25 GPa

Anke Wohlers [a,b,*], Craig E. Manning [b], Alan B. Thompson [a]

[a] *Institute of Geochemistry and Petrology, ETH Zurich, 8092 Zurich, Switzerland*
[b] *Department of Earth and Space Sciences, University of California, Los Angeles, CA 90095-1567, USA*

Received 1 September 2010; accepted in revised form 21 February 2011; available online 2 March 2011

Abstract

The solubilities of the assemblages albite + paragonite + quartz and jadeite + paragonite + quartz in H_2O were determined at 500 and 600 °C, 1.0–2.25 GPa, using hydrothermal piston-cylinder methods. The three minerals are isobarically and isothermally invariant in the presence of H_2O, so fluid composition is uniquely determined at each pressure and temperature. A phase-bracketing approach was used to achieve accurate solubility determinations. Albite + quartz and jadeite + quartz dissolve incongruently in H_2O, yielding residual paragonite which could not be retrieved and weighed. Solution composition fixed by the three-mineral assemblage at a given pressure and temperature was therefore bracketed by adding $NaSi_3O_{6.5}$ glass in successive experiments, until no paragonite was observed in run products. Solubilities derived from experiments bounding the appearance of paragonite thus constrain the equilibrium fluid composition. Results indicate that, at a given pressure, Na, Al, and Si concentrations are higher at 600 °C than at 500 °C. At both 500 and 600 °C, solubilities of all three elements increase with pressure in the albite stability field, to a maximum at the jadeite–albite–quartz equilibrium. In the jadeite stability field, element concentrations decline with continued pressure increase. At the solubility maximum, Na, Al, and Si concentrations are, respectively, 0.16, 0.05, and 0.48 molal at 500 °C, and 0.45, 0.27, and 1.56 molal at 600 °C. Bulk solubilities are 3.3 and 10.3 wt% oxides, respectively. Observed element concentrations are everywhere greater than those predicted from extrapolated thermodynamic data for simple ions, monomers, ion pairs, and the silica dimer. The measurements therefore require the presence of additional, polymerized Na–Al–Si-bearing species in the solutions. The excess solubility is >50% at all conditions, indicating that polymeric structures are the predominant solutes in the *P*–*T* region studied. The solubility patterns likely arise from combination of the large solid volume change associated with the albite–jadeite–quartz equilibrium and the rise in Na–Al–Si polymerization with approach to the hydrothermal melting curves of albite + quartz and jadeite + quartz. Our results indicate that polymerization of Na–Al–Si solutes is a fundamental aspect of fluid–rock interaction at high pressure. In addition, the data suggest that high-pressure metamorphic isograds can impose unexpected controls on metasomatic mass transfer, that significant metasomatic mass transfer prior to melting should be considered in migmatitic terranes, and that polymeric complexes may be an important transport agent in subduction zones.

1. INTRODUCTION

Aqueous fluids are responsible for substantial mass transfer in high pressure (*P*) and temperature (*T*) environments. For example, lithologies transported to deep-crustal conditions along Barrovian *P*–*T* paths show evidence for

* Corresponding author. Present address: German Research Centre for Geosciences (GFZ), Institute of Chemistry and Physics of Earth Materials, 14473 Potsdam, Germany. Tel.: +49 331 288 1828; fax: +49 331 288 1402.
E-mail address: Anke.Wohlers@gfz-potsdam.de (A. Wohlers).

0016-7037/$ - see front matter © 2011 Elsevier Ltd. All rights reserved.
doi:10.1016/j.gca.2011.02.028

significant compositional modification by metamorphic fluids (e.g., Ague, 1994a,b, 1995, 1997, 2003). Similarly, in subduction zones, slab devolatilization generates a fluid phase that is capable of major metasomatic activity (e.g., Manning, 2004).

Despite the important role that such fluids play in lower crustal and upper mantle processes, there are relatively few experimental determinations of their compositions at relevant P and T. Of particular importance is the determination of the solubility of key assemblages of rock-forming silicate minerals. However, experimental studies conducted on silicates in H_2O above 0.5 GPa chiefly focus on the solubility of a single mineral, such as quartz (Anderson and Burnham, 1965; Manning, 1994; Zotov and Keppler, 2000, 2002; Wang et al., 2004), albite (Anderson and Burnham, 1983; Stalder et al., 2000), zircon (Ayers and Watson, 1991; Newton et al., 2005, 2010), or Ca and Ca–Al silicates (Fockenberg et al., 2006, 2008; Newton and Manning, 2006, 2007). Notable exceptions targeted mantle bulk compositions or are reconnaissance in nature (Ryabchikov and Boettcher, 1980; Ryabchikov et al., 1982; Ryabchikov and MacKenzie, 1985; Schneider and Eggler, 1986; Zhang and Frantz, 2000; Newton and Manning, 2002). While such studies provide essential information, they offer limited insight into key solution properties like ionic strength, pH, and total dissolved solids in H_2O multiply saturated with crustal silicate minerals.

We experimentally determined the compositions of fluids in equilibrium with the assemblages albite + quartz + paragonite and jadeite + quartz + paragonite in H_2O, at 500 and 600 °C, 1.0–2.25 GPa. The two assemblages uniquely fix fluid composition, pH, ionic strength, and speciation at a given P and T in the system Na_2O–Al_2O_3–SiO_2–H_2O. These assemblages represent a useful model chemical system for the investigation of fluid–rock interaction involving granitic and pelitic mineral assemblages during high-P metamorphism. Moreover, combination of results on the two assemblages yields novel insights into solubility patterns near important reactions, including albite–jadeite–quartz equilibrium and hydrous melting of model crustal compositions.

2. METHODS

Minerals used as starting materials were natural, single crystals. We utilized low albite from Amelia Courthouse, jadeite from New Idria, California (Coleman, 1961), and high-purity Brazilian quartz (Manning, 1994). Electron microprobe analyses on 8 albite and 11 jadeite grains indicate the purity of both albite (<0.2 wt% CaO, <0.7 wt% K_2O, and <0.03 wt% FeO, MgO, TiO_2, Cr_2O_3, MnO) and jadeite (<0.3 wt% CaO, <0.6 wt% K_2O and <0.1 wt% FeO). In preparation for loading, single crystals were smoothed with sandpaper, cleaned in an ultrasonic bath, and dried at 300 °C. These measures helped ensure the mechanical integrity of each grain during an experiment. In addition to crystals, a quantity of $NaSi_3O_{6.5}$ glass (NS3) was added to most experiments. Glasses were prepared by first homogenizing a mixture of reagent-grade sodium carbonate and powdered Brazilian quartz by grinding in a mortar, and then pressing the mixture into a pellet. The pellet was decarbonated by slowly heating from 700 to 900 °C for 2 h, and then disaggregated and rehomogenized with a mortar and pestle. The powder was then melted at 1200 °C for 30 min and rapidly quenched to a crystal-free glass. This glass was added to experimental charges as small chips of a desired mass. Because the glass can be assumed to dissolve quickly and completely, this material proved useful for bringing the Na and Si concentration of the fluid closer to final values, which in turn limits mass loss from starting crystals, making them easier to manipulate and weigh after an experiment.

Experiments employed a double-capsule technique. A single albite or jadeite crystal, ~1 mm in the longest dimension and 2–5 mg in mass, was loaded into an inner Pt capsule of 1.5 mm outer diameter, which was then crimped at the ends to hold the crystal, and punctured with a needle to permit fluid circulation. This method allowed determination of the albite or jadeite weight loss by weighing the inner capsule before and after an experiment. The inner capsule was loaded into 1.8 cm long, 3.5 mm OD, 0.2 mm wall-thickness Pt capsule, along with a weighed quartz crystal, a quantity of $NaSi_3O_{6.5}$ glass, and 30–42 mg of ultrapure H_2O. The outer capsule was then crimped and sealed by arc welding. Welded seams of each capsule were carefully inspected for holes using a binocular microscope, and held at 110 °C for at least 2 h to check for leakage.

All experiments were conducted with a 2.54 cm diameter end-loaded piston-cylinder apparatus, with sodium chloride pressure medium and graphite furnaces (Manning and Boettcher, 1994). A flattened and folded capsule was placed transversely in a furnace, packed in NaCl, and covered with a 0.1 mm thick Pt foil to help prevent puncture by the thermocouple. At initiation of an experiment, pressure was increased to 0.8 GPa, followed by heating to 150 °C to prevent H_2O freezing. Then pressure and temperature were increased together to desired run conditions. Temperature was maintained to within ±1 °C using Pt–$Pt_{90}Rh_{10}$ thermocouples accurate to within ±3 °C. No corrections were made for the effect of pressure on emf. Pressure was measured with a Heise bourdon-tube gauge, considered accurate to ±300 bars. At termination, experiments were quenched to <50 °C in <1 min, then extracted from the furnace, weighed, pierced with a needle and dried for 20 min at 110 °C to determine the H_2O content by weight loss of the capsule. Run products were removed from the capsules, cleaned and weighed.

The method for solubility determination differed from that of Manning et al. (2010), where fluid composition was established either by analysis of quench fluid or by a weight-loss mass-balance method, in which albite was weighed before and after removal of the paragonite coating. The latter approach required a correction for quench solutes. At the high solubilities of the present study, the weight-loss approach would nominally be appropriate, but albite and jadeite proved to be highly friable, and newly grown paragonite often sifted off of the starting-crystal surface prior to weighing. Thus, although an inner capsule weight change corresponding to the extent of the reaction albite or jadeite + H_2O → paragonite + solutes could be determined, the individual masses of albite, jadeite and paragonite could not.

Solubilities were instead determined by a bracketing method. The mass of NS3 was varied in successive experiments at a given P and T to constrain paragonite saturation. The composition of the fluid coexisting with albite/jadeite + paragonite + quartz is bracketed between the paragonite-bearing run with the least NS3, and the paragonite-free run with the most NS3. Weight changes of quartz and the inner capsule in paragonite-free runs directly determine minimum Al solubility and maximum Na, Si, and bulk solubility. In contrast, in paragonite-bearing experiments, the inner capsule and quartz weight changes combined with the NS3 glass weight constrain the maximum Al concentration and the minimum bulk, Na and Si solubilities. All solubility calculations employed the H_2O mass determined before each experiment. Checks on the H_2O after an experiment gave slightly lower weights, consistent with minor uptake by paragonite. Moreover, H_2O loss to paragonite tends to zero where the mineral saturates because its mass by definition becomes infinitesimally small.

Weights of inner-capsules, glass and crystals were determined on a Mettler UMX2 ultra-microbalance, with a precision of 0.2 μg (1σ). H_2O was weighed on a Mettler M3 microbalance ($1\sigma = 2$ μg). Crystals were studied by optical and scanning-electron microscopy. In addition, selected paragonite grains were analyzed by electron microprobe.

3. RESULTS

Results are given in Table 1. All NS3 glass dissolved completely. Quench material on residual crystals was negligible. In the presence of quartz, albite and jadeite dissolved incongruently in H_2O to paragonite + solutes (Fig. 1A and B), unless sufficient NS3 glass had been added to suppress the mica. Paragonite, confirmed by electron microprobe analysis, grew as $\leqslant$10 μm, euhedral hexagonal platelets on albite and jadeite surfaces (Fig. 1C and D). Paragonite was found only in the inner capsule, confirming that it was not a quench product in the experiments in which it grew, but rather a stable product of reaction consistent with its stability field (e.g., Chatterjee, 1972). In experiments in which sufficient NS3 glass was added to suppress paragonite growth, the albite or jadeite crystal surfaces were clean and exhibited textural features consistent with strong dissolution, such as pits and grooves (Fig. 1E and F). Quartz crystals became faceted during partial dissolution. No sign of melting was observed, consistent with the results of Boettcher and Wyllie (1969), who found hydrothermal melting of albite + quartz and jadeite + quartz at ~650–700 °C at the pressures of our study.

Experiment durations were 42–144 h at 500 °C, and 12–45 h at 600 °C. Results at 500 °C, 1 GPa, are consistent with Manning et al. (2010) (see below). This and the absence of any time-dependent inconsistency in the data set (Table 1) support the assumption of attainment of equilibrium.

Errors were propagated from weighing uncertainties. Maximum values of 2σ, as a percentage of an individual determination, are 0.50% (bulk solubility), 0.37% (Al), 0.14% (Na), and 0.19% (Si). These are in all cases smaller than the symbol sizes in Fig. 2.

Paragonite saturation was bracketed at nine discrete P–T conditions (Fig. 2). At a given P and T, Bulk, Na and Si solubilities were, with one exception lower when paragonite was present than when it was absent, while Al was higher, consistent with the amount of NS3 glass added to locate the paragonite saturation point. A minor solubility "cross-over" occurred at 500 °C, 1.75 GPa, in which the maximum Si and bulk solubilities in paragonite-free experiments are slightly lower than the minimum values implied by the paragonite-present experiments. However, the magnitude of the crossover is small, and Na and Al do not show the same effect. At 500 °C and 600 °C, bulk and individual element solubilities in H_2O in equilibrium with albite + quartz + paragonite increase with increasing pressure. In contrast, bulk and individual element solubilities of jadeite + quartz + paragonite decrease as pressure rises. Extrapolation of the trends to their intersections gives the position of the equilibrium (Fig. 2D)

$$\underset{\text{albite}}{NaAlSi_3O_8} = \underset{\text{jadeite}}{NaAlSi_2O_6} + \underset{\text{quartz}}{SiO_2} \tag{1}$$

The bulk solubility maximum at this point corresponds to ~3.3 wt% oxides at 500 °C, and ~10.3 wt% oxides at 600 °C (Fig. 2D); individual element trends similarly exhibit maxima at the position of Eq. (1) at each T.

Table 2 gives the midpoint of each isothermal, isobaric solubility bracket. Listed uncertainties are 1σ, assuming a uniform distribution of solubility between the limiting experiments. At each T, the mass of NS3 glass required to suppress paragonite increased with P (Table 1). The fluid phase is therefore peralkaline at all investigated conditions, and Na/Al (molar) increases with P (Fig. 3), attaining maximum values of 3.2 at 500 °C and 2.4 at 600 °C. The Na/Al ratio does not show a resolvable break in slope at Eq. (1). Fluids at all investigated conditions contain more Si than either Na or Al, and the molar Si/(Na + Al) ratio is ~2.5. Thus, the fluids everywhere possess a stoichiometry more silicic than that of albite, in which the ratio is 1.5.

4. DISCUSSION

4.1. Comparison to previous work

4.1.1. Incongruent dissolution of albite and jadeite at quartz saturation

Previous studies have shown that albite dissolution in H_2O is incongruent over a wide range of metamorphic P and T (e.g., Morey and Hesselgesser, 1951; Morey and Chen, 1955; Hemley et al., 1961; Currie, 1968; Anderson and Burnham, 1983; Stalder et al., 2000; Shmulovich et al., 2001). Ryabchikov and MacKenzie (1985) found that, at 650 °C, jadeite dissolved congruently in H_2O at 2.0 GPa, but incongruently to diaspore + solutes at 3.0 GPa. Our results at 500 and 600 °C indicate that both albite and jadeite also dissolve incongruently in H_2O in the presence of excess quartz, yielding residual paragonite + solutes. This agrees with the study of Woodland and Walther (1987) and Manning et al. (2010).

Table 1
Experimental results.

Run	Time (h)	T (°C)	P (GPa)	H_2O in (mg)	IC in (mg)	IC out (mg)	qz in (mg)	qz out (mg)	NS3 (mg)	m_{Al} (mol/kg)	m_{Na} (mol/kg)	m_{Si} (mol/kg)	Bulk (wt%)	Products
Ab51	51	500	1.00	32.224	57.7706	57.3206	0.9234	0.7659	0.000	0.053	0.053	0.241	1.85	ab, qz, pg
Ab52	46	500	1.00	31.399	54.8644	54.5502	0.7504	0.5902	0.187	0.038	0.066	0.284	2.06	ab, qz, pg
Ab59	95	500	1.00	38.498	61.1864	60.8046	2.3604	2.1581	0.201	0.038	0.062	0.275	2.00	ab, qz, pg
Ab50	48	500	1.00	31.300	56.0681	55.8296	1.5051	1.4161	0.350	0.029	0.082	0.293	2.12	ab, qz
Ab53	48	500	1.45	39.201	55.3210	54.5920	1.1061	1.1329	0.212	0.071	0.096	0.278	2.28	ab, qz, pg
Ab54	92	500	1.45	40.534	54.5441	53.9440	1.3221	1.3422	0.734	0.056	0.142	0.418	3.14	ab, qz, pg
Ab58	46	500	1.45	41.850	56.6063	56.0977	2.5272	2.5436	0.942	0.046	0.153	0.452	3.31	ab, qz
Ab55	49	500	1.45	40.069	60.8618	60.4698	1.1326	1.0374	1.038	0.037	0.160	0.519	3.67	ab, qz
Jd31	46	500	1.55	33.243	61.8303	61.4364	7.7727	7.6206	0.543	0.059	0.136	0.425	3.17	jd, qz, pg
Jd62	49	500	1.55	36.690	64.4803	64.0784	1.0957	0.9002	0.659	0.054	0.139	0.452	3.31	jd, qz, pg
Jd61	54	500	1.55	32.778	51.3835	51.0819	1.1197	1.0364	0.811	0.046	0.163	0.485	3.52	jd, qz
Jd30	42	500	1.55	39.380	67.2221	66.9431	7.7222	7.7728	1.200	0.035	0.179	0.481	3.50	jd, qz
Jd60	125	500	1.75	37.701	56.9886	56.4658	1.3414	1.1209	0.454	0.069	0.126	0.405	3.08	jd, qz, pg
Jd 63	144	500	1.75	40.450	63.7561	63.3467	1.0106	0.9059	0.670	0.050	0.128	0.378	2.84	jd, qz, pg
Jd66	72.0	500	1.75	33.405	81.6136	81.3506	1.2725	1.3295	0.806	0.039	0.153	0.392	2.94	jd, qz
Jd65	76	500	1.75	30.900	69.5580	69.4065	1.0487	1.2725	1.208	0.024	0.209	0.483	3.55	jd, qz
Ab36	21	600	1.20	39.224	56.2581	54.5484	2.1565	1.4048	0.161	0.166	0.186	0.876	6.27	ab, qz, pg
Ab35	21	600	1.20	30.296	59.8367	58.6091	3.0302	2.4539	0.318	0.155	0.204	0.929	6.54	ab, qz, pg
Ab34	22	600	1.20	39.763	59.2193	57.6280	2.8976	2.1598	0.592	0.153	0.223	0.978	6.84	ab, qz
Ab30	26	600	1.20	35.799	58.6452	57.5119	4.3759	4.0089	1.215	0.121	0.281	1.015	7.05	ab, qz
Ab1	20	600	1.55	39.876	65.9674	63.0842	1.1866	0.2680	0.000	0.276	0.276	1.211	8.70	ab, qz, pg
Ab4	15	600	1.55	40.099	72.4968	69.8963	1.1562	0.6253	1.275	0.247	0.398	1.414	9.90	ab, qz, pg
Ab3	23	600	1.55	39.760	67.5757	65.0567	1.5901	1.1664	1.562	0.242	0.428	1.460	10.18	ab, qz
Ab2	19	600	1.55	39.672	69.8893	67.4974	2.0041	1.5901	1.725	0.230	0.436	1.481	10.25	ab, qz
Jd14	22	600	1.75	32.502	64.0003	62.0450	2.3597	1.3069	0.464	0.298	0.365	1.337	9.65	jd, qz, pg
Jd12	32	600	1.75	29.510	59.0436	57.4888	5.8630	5.0124	0.855	0.261	0.398	1.413	9.95	jd, qz, pg
Jd13	14	600	1.75	32.524	66.0725	64.4285	3.4817	2.5597	1.089	0.250	0.409	1.448	10.10	jd, qz, pg
Jd10	45	600	1.75	38.298	62.5877	60.6684	4.2263	2.9954	1.592	0.248	0.445	1.621	11.02	jd, qz
Jd16	21	600	1.75	38.794	64.3545	62.4937	4.5322	3.2260	1.683	0.237	0.443	1.651	11.11	jd, qz
Jd2	23	600	2.00	29.904	63.8798	62.5572	6.0002	5.0164	0.552	0.219	0.306	1.247	8.72	jd, qz, pg
Jd4	22	600	2.00	37.886	66.3833	64.8934	5.9848	4.6805	1.004	0.195	0.320	1.338	9.11	jd, qz, pg
Jd7	14	600	2.00	39.171	65.3423	63.8266	3.5913	2.3982	1.324	0.191	0.351	1.370	9.34	jd, qz, pg
Jd6	12	600	2.00	37.616	61.7008	60.3742	7.2296	6.3791	1.773	0.174	0.398	1.395	9.50	jd, qz
Jd32	21	600	2.25	40.467	59.4203	57.5608	2.4538	1.0756	0.543	0.227	0.291	1.212	8.54	jd, qz, pg
Jd36	22	600	2.25	38.311	63.9585	62.5298	2.7846	1.6435	1.026	0.184	0.311	1.245	8.58	jd, qz, pg
Jd33	22	600	2.25	38.781	63.3174	62.1310	1.4045	0.3920	1.395	0.151	0.322	1.248	8.48	jd, qz, pg
Jd35	19	600	2.25	39.806	58.6208	57.4365	1.8419	0.9234	1.597	0.147	0.337	1.248	8.50	jd, qz, pg
Jd34	21	600	2.25	39.181	56.6099	55.5159	1.0758	0.2674	1.810	0.138	0.357	1.276	8.65	jd, qz

Abbreviations: IC, inner capsule; NS3, $NaSi_3O_{6.5}$ glass; qz, quartz; ab, albite; jd, jadeite; pg, paragonite. "In" and "out" refer, respectively, to a weight before and after experiment. H_2O added with a micro syringe and weight before experiment was used for fluid composition calculation. Bulk solubility is wt% $SiO_2 + AlO_{1.5} + NaO_{0.5}$. Weights reported to three decimal places were determined on a Mettler M3 microbalance ($1\sigma = 2$ μg), whereas those reported to four places were determined on a Mettler UMX2 ultramicrobalance ($1\sigma = 0.2$ μg). Propagation of weighing errors to solubilities gave average 1σ in bulk solubility, m_{Al}, m_{Na}, m_{Si} of respectively 2.2e−3, 3.6e−5, 4.5e−5 and 2.3e−4.

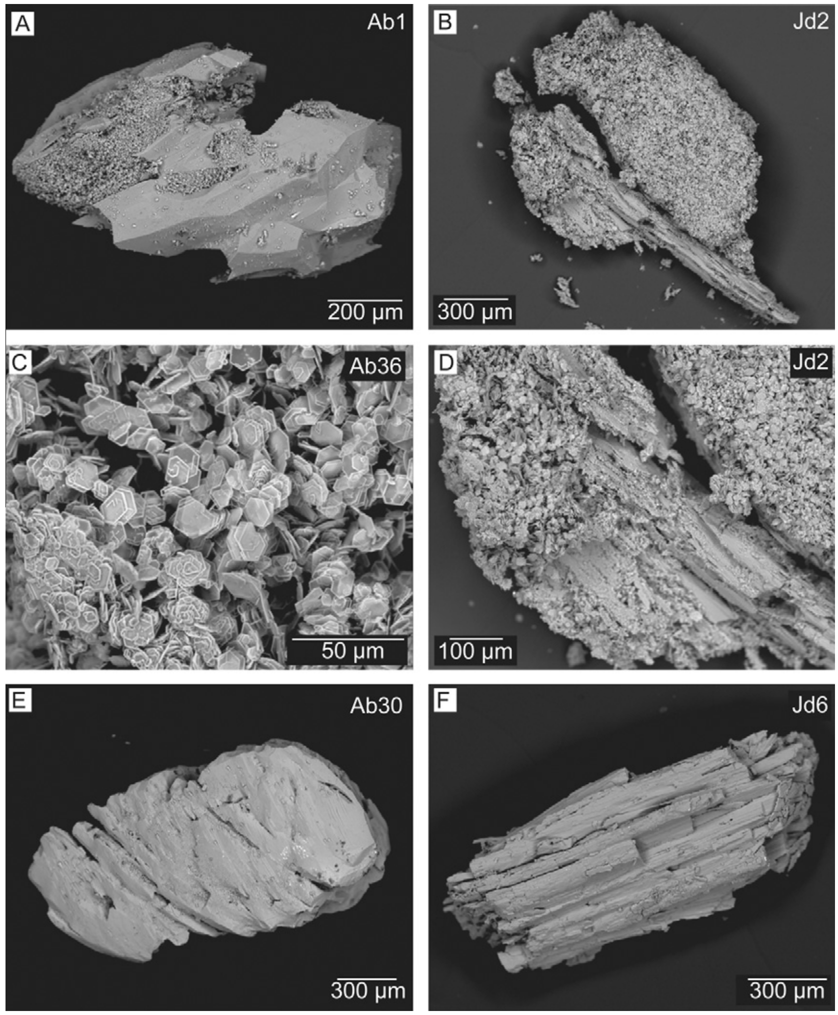

Fig. 1. Back-scattered electron images of experimental run products. (A) Albite crystal partially covered with paragonite at 600 °C and 1.55 GPa. (B) Jadeite almost completely covered in paragonite for an experiment at 600 °C and 2 GPa. Panel (D) shows and enlarged area of (B). Panels (C) and (D) show platy paragonite flakes. Panels (E) and (F) illustrate the results of adding sufficient $NaSi_3O_{6.5}$ glass to suppress the growth of paragonite on albite (E) and jadeite (F).

The variation in incongruent dissolution of albite and jadeite (±quartz) can be assessed using molar Na/Al ratios of solutes (Fig. 3A). Previous studies of albite dissolution in H_2O, without quartz and below 0.8 GPa, suggest a weak dependence of Na/Al on P at 500 and 600 °C (Morey and Hesselgesser, 1951; Currie, 1968; Anderson and Burnham, 1983). The Na/Al ratios from Manning et al. (2010) at 1 GPa are higher than those at lower P, in agreement with predictions of Antignano and Manning (2008). Our data indicate further isothermal increases in Na/Al with P that are broadly consistent with previous work.

Taken together, data on the solubility of albite or albite/jadeite–paragonite–quartz show that dissolution becomes progressively more incongruent as P increases. At a given P, peralkalinity decreases with increasing T, indicating a larger increase in Al relative to Na solubility as T rises. Thus, at T higher than our study, our data predict an approach to congruent dissolution behavior. This would likely explain why, at 650 °C, Ryabchikov and MacKenzie (1985) found that jadeite dissolves congruently in H_2O at 2.0 GPa, but incongruently at 3.0 GPa.

4.1.2. Solubility

Manning et al. (2010) determined albite–paragonite–quartz solubility at 1.0 GPa, 350–620 °C, by direct analysis of quenched fluid and weight-loss methods. Fig. 3B shows that, despite the different methods employed, our bulk-solubility data at 500 °C agree closely with their results. Similar agreement is seen for individual elements.

Previous work on Si concentrations in H_2O in equilibrium with either quartz or albite alone indicates rising solubility with P at both temperatures (Fig. 4). Fig. 4A shows that the solubility of quartz in H_2O (in the absence of albite or jadeite) increases with P at both temperatures (Manning, 1994). Similarly, albite dissolution in H_2O (in the absence of quartz) yields increasing Si concentration with P (Fig. 4B; Morey and Hesselgesser, 1951; Currie, 1968; Anderson and Burnham, 1983). Extrapolation of the albite solubility

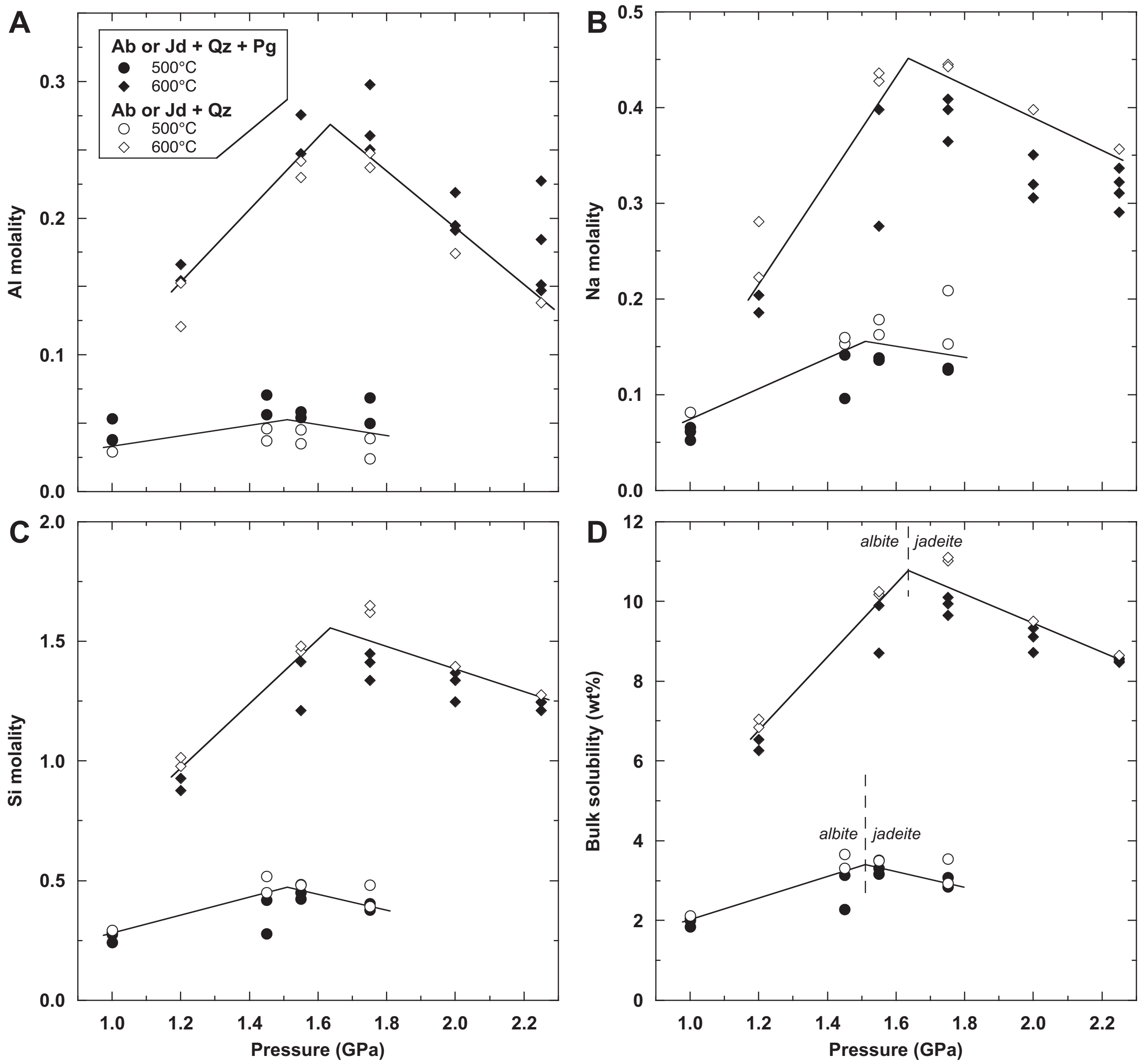

Fig. 2. Experimentally constrained concentrations of aluminum (A), sodium (B), silica (C) (mol/kg H_2O) and bulk solubility (D) (wt%) at 500 °C (circles) and 600 °C (diamonds). Open symbols indicate experiments without paragonite; filled symbols denote paragonite-bearing runs. At a given P and T, the fluid composition in equilibrium with albite/jadeite + paragonite + quartz must lie between the two types of experiment (see text), as illustrated by the solid lines. Individual element concentrations and bulk solubility increase from 1 GPa to the albite–jadeite–quartz equilibrium (vertical dashed lines in panel (D)); concentrations decline at higher P. Propagated 2σ errors in solubility (Table 1) are smaller than symbol size.

Table 2
Fluid compositions coexisting with quartz + paragonite + albite or jadeite.

P (GPa)	T (°C)	Mineral assemblage	Bulk solubility (wt%)	Si (mol/kg H_2O)	Al (mol/kg H_2O)	Na (mol/kg H_2O)	Na/Al (M)
1.00	500	APQ	2.058(35)	0.284(05)	0.033(03)	0.072(06)	2.16(23)
1.45	500	APQ	3.226(50)	0.435(10)	0.051(03)	0.148(03)	2.87(17)
1.55	500	JPQ	3.415(61)	0.468(09)	0.050(03)	0.151(07)	3.03(20)
1.75	500	JPQ	2.891(28)	0.385(04)	0.045(03)	0.141(07)	3.16(28)
1.20	600	APQ	6.694(86)	0.954(14)	0.154(01)	0.214(05)	1.39(04)
1.55	600	APQ	10.039(79)	1.437(13)	0.244(02)	0.413(09)	1.69(04)
1.75	600	JPQ	10.561(264)	1.534(50)	0.249(01)	0.427(10)	1.71(04)
2.00	600	JPQ	9.419(49)	1.382(07)	0.183(05)	0.375(13)	2.05(09)
2.25	600	JPQ	8.579(44)	1.262(08)	0.143(03)	0.347(06)	2.43(06)

Fluid compositions are midpoints between bracketing solubilities. Parenthetical numbers reflect 1σ in the final digits, calculated assuming equal probability of solubility between limiting values. *Abbreviations:* A, albite; J, jadeite; P, paragonite; Q, quartz.

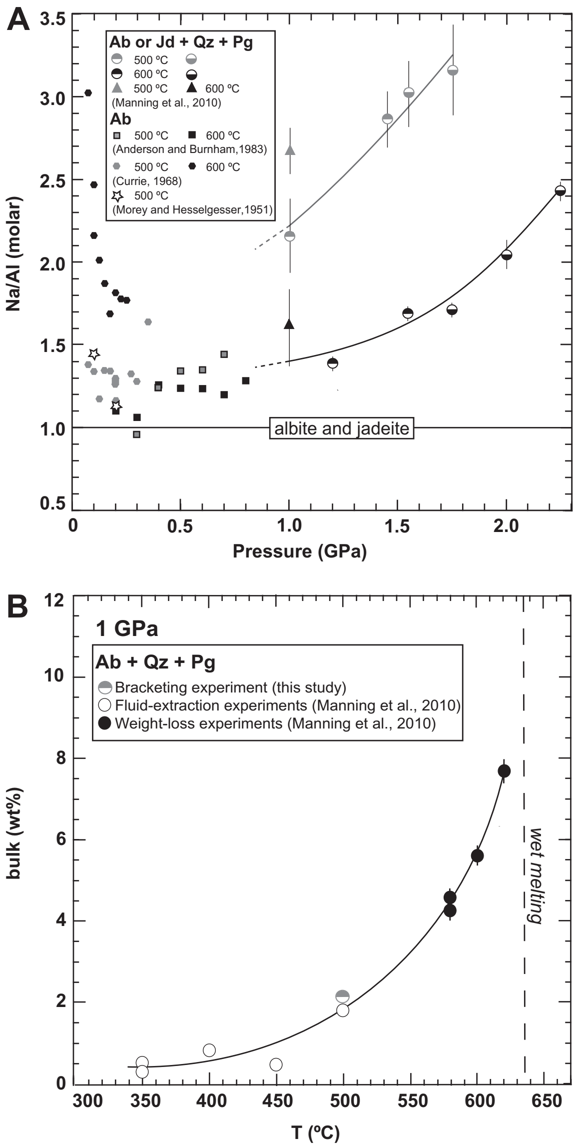

Fig. 3. (A) Comparison of the variation in the molar Na/Al ratio with pressure at 500 °C (gray) and 600 °C (black) (Morey and Hesselgesser, 1951; Currie, 1968; Anderson and Burnham, 1983; Manning et al., 2010; this study). At both temperatures, fluids become progressively enriched in Na relative to Al with increasing *P*. At a given *P*, molar Na/Al ratios decrease toward unity (i.e., congruent albite or jadeite dissolution) with increasing *T*. (B) Comparison of bulk solubility of albite + paragonite + quartz in H_2O at 1 GPa (Manning et al., 2010; this study). Despite different experimental methods, the two studies show excellent agreement.

results to higher *P* suggests that Si content of albite-saturated H_2O would exceed that of quartz-saturated H_2O at higher *P* than those investigated. Our results demonstrate that when albite or jadeite and quartz are present together, along with the incongruent product paragonite, the total Si in solution is significantly higher than in the presence of albite or quartz alone. The elevation of Si solubility well above that in H_2O saturated with a single mineral (quartz or albite) strongly suggests that Si complexes with other elements in solution (see below).

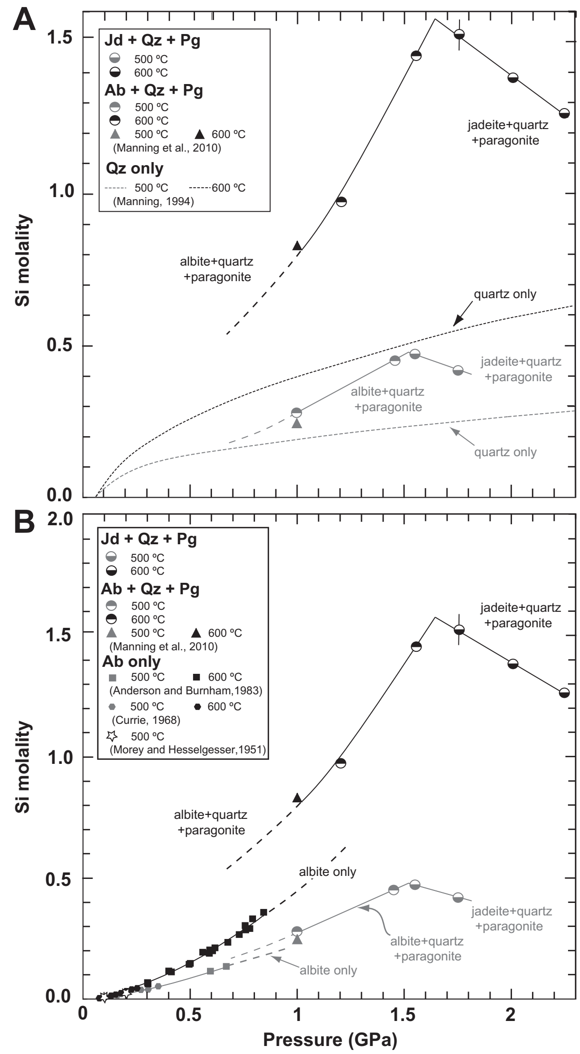

Fig. 4. Comparison of Si concentrations in the presence of albite/jadeite + quartz + paragonite (Manning et al., 2010; this work) to (A) previous results on quartz solubility in H_2O without albite (Manning, 1994) and (B) albite solubility in H_2O without quartz (Morey and Hesselgesser, 1951; Currie, 1968; Anderson and Burnham, 1983). The silica concentrations in the presence ab or jd + pg + qtz are higher then that predicted by extrapolations of the albite-only results of Anderson and Burnham (1983).

Our data indicate that bulk and individual-element solubilities in the jadeite stability field decrease with *P* at 500 and 600 °C. Ryabchikov and MacKenzie (1985) obtained a similar result for bulk jadeite solubility in H_2O at 650 °C, 2.0 and 3.0 GPa.

4.1.3. Albite–jadeite–quartz equilibrium

The different signs of the *P* dependence of solubility in the albite and jadeite stability fields indicate that the solubility data offer a novel means of bracketing the position of Eq. (1). Linear extrapolations of our results within each stability field must intersect at the *P* of Eq. (1) at a given *T*. The data at 600 °C suggest an equilibrium *P* of 1.64 GPa, identical to the results of Hays and Bell (1973) and Holland

(1980) despite their use of synthetic high albite. Our result of 1.51 GPa at 500 °C is the first experimental constraint at this T. The intersections at both T differ slightly from predictions based on the Holland and Powell (1998) data set (2002 update), which gives equilibrium P of 1.43 and 1.67 GPa at 500 and 600 °C, respectively. The small differences in the implied position of Eq. (1) may simply be due to our use of natural low-albite and jadeite.

4.2. Comparison to predicted fluid composition

The experimental results document an isothermal rise and then decline of measured element concentrations near the albite–jadeite–quartz transition. The origins of these pressure-dependent changes in solubility can be explored via comparison of measured fluid compositions with those calculated from thermodynamic data.

4.2.1. Prediction of fluid composition and speciation

Species abundance and fluid composition were calculated at experimental conditions following the approach of Manning et al. (2010). The assemblages albite + paragonite + quartz and jadeite + paragonite + quartz in pure H_2O buffer pH at values greater than acid–base neutrality. Therefore, the acidic species Al^{+3}, $AlOH^{+2}$ and AlO^{+} may be assumed negligible, giving a set of 11 species: the neutral species $HAlO_{2,aq}$, $NaOH_{aq}$, $NaAlO_{2,aq}$, $NaHSiO_{3,aq}$, $SiO_{2,aq}$, and $Si_2O_{4,aq}$, and the ionic species H^+, OH^-, Na^+, AlO_2^- and $HSiO_3^-$. Silica species notation follows Newton and Manning (2002, 2003, 2008); others are after Shock et al. (1997) and Sverjensky et al. (1997). The equations used to calculate fluid composition and speciation are given in Appendix.

Table 3 gives the computational results at the experimentally investigated P and T. For each P and T, fluid composition was computed by initially setting $I = 0$, calculating activity coefficients and species abundances, then updating I and repeating. Solutions converged in less than ten iterations. Calculated pH is alkaline in every case, supporting our assumption of negligible Al^{+3}, $AlOH^{+2}$, and AlO^{+}. Ion activity coefficients ranged from 0.6 to 0.7, and predicted ionic strength was everywhere <0.1.

4.2.2. Measured vs. predicted fluid compositions

Fig. 5 and Table 4 compare predicted and observed bulk solubility and individual element concentrations. At each P–T studied, measured solubility is greater than that calculated from thermodynamic data. Manning et al. (2010) found

Table 3
Log K values and calculation results.

T (°C):	500	500	500	500	600	600	600	600	600	600
P (GPa):	1	1.45	1.55	1.75	1	1.2	1.55	1.75	2	2.25
log K values										
(1) $3Ab + 2H^+ = Pg + 6Qz + 2Na^+$	9.548	9.833	–	–	9.149	9.277	9.455	–	–	–
(2) $Ab + 2AlO_2^- + 2H^+ = Pg$	17.034	16.424	–	–	16.110	15.751	15.255	–	–	–
(3) $3Jd + 2H^+ = Pg + 3Qz + 2Na^+$	–	–	9.484	8.928	–	–	–	9.298	8.673	8.046
(4) $Jd + Qz + 2AlO_2^- + 2H^+ = Pg$	–	–	16.185	15.767	–	–	–	14.938	14.445	13.982
(5) $H_2O = H^+ + OH^-$	−8.407	−7.939	−7.858	−7.703	−8.408	−8.160	−7.816	−7.652	−7.476	−7.319
(6) $Qz + H_2O = HSiO_3^- + H^+$	−8.656	−8.112	−8.018	−7.838	−8.991	−8.718	−8.339	−8.159	−7.965	−7.792
(7) $HAlO_{2,aq} = H^+ + AlO_2^-$	−4.403	−4.161	−4.119	−4.039	−4.605	−4.465	−4.271	−4.179	−4.080	−3.991
(8) $NaOH_{aq} = Na^+ + OH^-$	0.196	0.641	0.719	0.866	0.031	0.309	0.695	0.878	1.075	1.252
(9) $NaAlO_{2,aq} = Na^+ + AlO_2^-$	−0.478	−0.115	−0.051	0.069	−0.664	−0.448	−0.148	−0.006	0.148	0.285
(10) $Qz + NaOH_{aq} = NaHSiO_{3,aq}$	−0.258	−0.044	−0.007	0.063	−0.888	−0.771	−0.609	−0.532	−0.449	−0.375
(11) $Qz = SiO_{2,aq}$	−0.868	−0.764	−0.745	−0.709	−0.674	−0.612	−0.519	−0.471	−0.417	−0.367
(12) $SiO_{2,aq} = Si_2O_{4,aq}$	0.108	−0.130	−0.183	−0.289	0.305	0.199	0.014	−0.092	−0.225	−0.357
Calculation results										
I	0.033	0.072	0.067	0.058	0.032	0.047	0.080	0.090	0.079	0.067
γ_1	0.701	0.615	0.623	0.639	0.704	0.664	0.602	0.587	0.604	0.622
pH	6.406	6.237	6.121	5.894	6.218	6.147	6.045	5.924	5.659	5.401
log[H_+]	−6.252	−6.025	−5.916	−5.700	−6.066	−5.969	−5.824	−5.693	−5.440	−5.195
log[OH^-]	−1.847	−1.491	−1.531	−1.615	−2.038	−1.836	−1.551	−1.497	−1.598	−1.712
log[AlO_2^-]	−1.957	−1.752	−1.766	−1.795	−1.684	−1.551	−1.362	−1.314	−1.344	−1.384
log[Na^+]	−1.477	−1.145	−1.174	−1.236	−1.492	−1.330	−1.097	−1.044	−1.104	−1.172
log[$HAlO_{2,aq}$]	−4.114	−4.039	−3.974	−3.845	−3.450	−3.411	−3.356	−3.290	−3.143	−3.000
log[$NaOH_{aq}$]	−3.829	−3.699	−3.834	−4.105	−3.865	−3.831	−3.784	−3.882	−4.215	−4.548
log[$NaAlO_{2,aq}$]	−3.264	−3.205	−3.299	−3.488	−2.816	−2.789	−2.752	−2.814	−3.034	−3.252
log[$SiO_{2,aq}$]	−0.868	−0.764	−0.745	−0.709	−0.674	−0.612	−0.519	−0.471	−0.417	−0.367
log[$Si_2O_{4,aq}$]	−1.628	−1.659	−1.673	−1.707	−1.043	−1.025	−1.024	−1.034	−1.058	−1.091
log[$HSiO_3^-$]	−2.096	−1.664	−1.691	−1.750	−2.620	−2.393	−2.074	−2.004	−2.087	−2.185
log[$NaHSiO_{3,aq}$]	−4.087	−3.744	−3.841	−4.041	−4.753	−4.602	−4.393	−4.414	−4.665	−4.922
log[Na_{total}]	−1.467	−1.139	−1.169	−1.232	−1.469	−1.314	−1.086	−1.036	−1.098	−1.168
log[Al_{total}]	−1.933	−1.735	−1.750	−1.783	−1.647	−1.521	−1.341	−1.296	−1.329	−1.368
log[Si_{total}]	−0.719	−0.624	−0.615	−0.598	−0.403	−0.360	−0.300	−0.273	−0.247	−0.223
Bulk solubility (oxide wt%)	1.295	1.718	1.729	1.752	2.529	2.845	3.378	3.611	3.744	3.871

Abbreviations: Ab (albite), Jd (jadeite), Pg (paragonite), Qz (quartz). Square brackets denote concentration in molal.

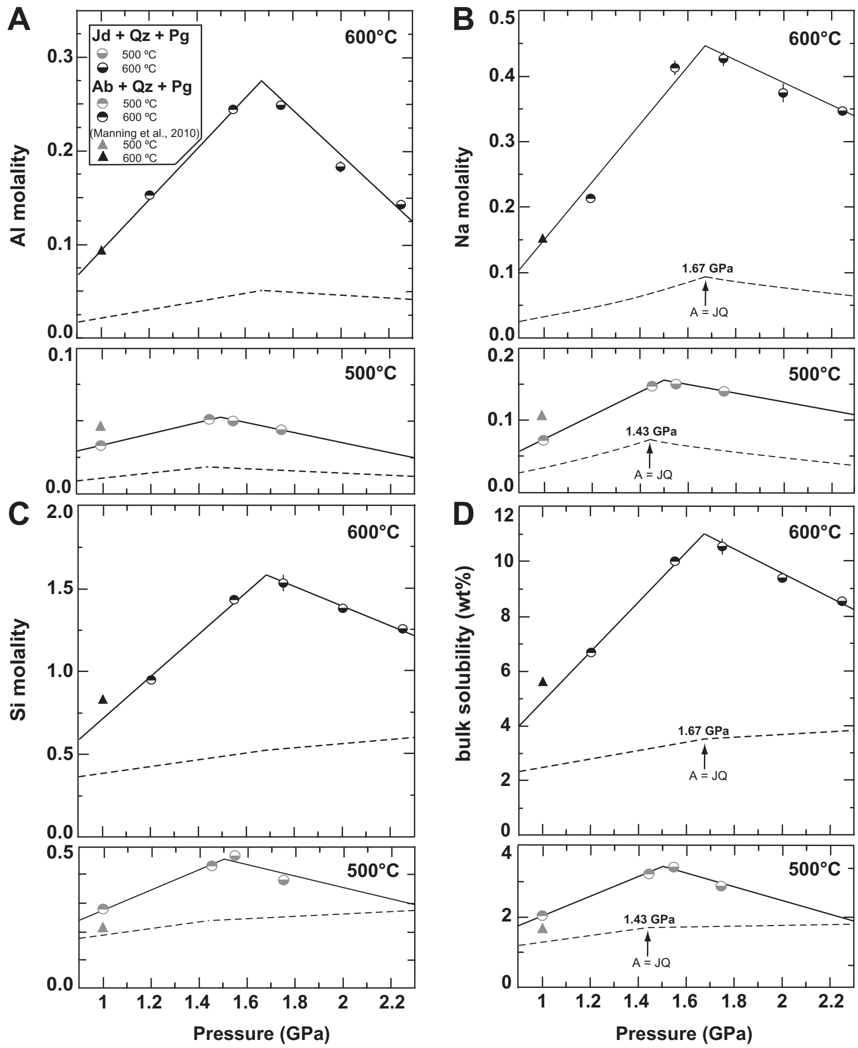

Fig. 5. Measured vs. predicted concentrations of Al (A), Na (B), Si (C) and bulk solutes (D) in H_2O in the presence of albite or jadeite + quartz + paragonite. Symbols as in Fig. 4. Predicted element concentrations (dashed lines) are lower than measured values (solid lines) at all investigated temperatures and pressures. Predicted and measured aluminum and sodium concentrations in the fluids increase to a maximum at the albite = jadeite + quartz transition, and then decrease with further increase in P in the jadeite stability field. Predicted silica concentrations and bulk solubility increases over the whole pressure range, whereas measured values increase to the transition, followed by solubility decrease.

that, at 1 GPa, predicted and measured solubilities of albite + paragonite + quartz in H_2O agreed at $\leqslant$450 °C; however, with increasing T, observed solubility became progressively greater than that calculated, up to the point of hydrothermal melting. Our result at 500 °C, 1 GPa, is consistent with this analysis, and they suggest that similar isobaric trends occur at all investigated P. In the albite stability field, increasing P at constant T yields widening excesses in measured bulk and individual element solubilities, with greater excess solubility at 600 °C than at 500 °C. The trend continues until jadeite becomes stable. In the jadeite stability field, measured bulk and individual element solubilities decline with a further rise P at constant T. The maximum excess bulk, Si, Al, and Na solubilities occur at the albite–jadeite–quartz equilibrium boundary at each T. If the trends are linear, then agreement between measured and predicted solubility is implied at <1.0 GPa and >2.25 GPa.

Element ratios in the experimental fluids also differ from those calculated (Fig. 6A, B and Table 4). The experimentally constrained bulk solutes possess lower Si/(Na + Al) than thermodynamic data would indicate. The calculations suggest that, at a given P, the fluid composition should become more Si rich with rising T. However, the experiments reveal that element ratios in the fluids are not strongly sensitive to T in the range 500–600 °C: Al is $\sim$10 ± 2 mol%, and Na + Al is $\sim$30 ± 5 mol% over the investigated range of conditions.

4.3. Origin of excess solubility

The experimental fluids possess concentrations of Na, Al and Si that are significantly greater than those predicted (Table 4 and Fig. 5). The solubility excesses could arise from experimental methodology or inaccurate thermody-

Table 4
Composition of solute fractions (oxide wt%).

	APQ 500 °C 1.00 GPa	APQ 500 °C 1.45 GPa	JPQ 500 °C 1.55 GPa	JPQ 500 °C 1.75 GPa	APQ 600 °C 1.00 GPa	APQ 600 °C 1.20 GPa	APQ 600 °C 1.55 GPa	JPQ 600 °C 1.75 GPa	JPQ 600 °C 2.00 GPa	JPQ 600 °C 2.25 GPa
Observed										
$NaO_{0.5}$	0.219	0.442	0.452	0.424	0.443	0.618	1.151	1.183	1.051	0.983
$AlO_{1.5}$	0.167	0.254	0.245	0.220	0.448	0.731	1.121	1.135	0.845	0.665
SiO_2	1.672	2.531	2.718	2.247	4.729	5.346	7.767	8.246	7.523	6.931
Bulk	2.058	3.227	3.415	2.891	5.620	6.695	10.039	10.564	9.419	8.579
Predicted										
$NaO_{0.5}$	0.104	0.221	0.207	0.178	0.102	0.146	0.245	0.275	0.238	0.202
$AlO_{1.5}$	0.059	0.092	0.089	0.083	0.112	0.149	0.225	0.249	0.230	0.210
SiO_2	1.132	1.404	1.434	1.491	2.314	2.550	2.907	3.088	3.275	3.458
Bulk	1.295	1.718	1.729	1.752	2.529	2.845	3.378	3.611	3.744	3.871
Excess										
$NaO_{0.5}$	0.115	0.221	0.245	0.245	0.340	0.472	0.905	0.908	0.814	0.781
$AlO_{1.5}$	0.108	0.161	0.156	0.138	0.336	0.581	0.896	0.887	0.615	0.455
SiO_2	0.540	1.126	1.285	0.756	2.415	2.796	4.860	5.158	4.248	3.473
Bulk	0.763	1.508	1.686	1.139	3.091	3.849	6.661	6.953	5.677	4.709
Polymerized										
$NaO_{0.5}$	0.115	0.221	0.245	0.245	0.340	0.472	0.905	0.908	0.814	0.781
$AlO_{1.5}$	0.108	0.161	0.156	0.138	0.336	0.581	0.896	0.887	0.615	0.455
SiO_2	0.820	1.386	1.535	0.988	3.475	3.897	5.959	6.229	5.260	4.411
Bulk	1.043	1.768	1.937	1.371	4.151	4.950	7.760	8.024	6.689	5.647
Unpolymerized										
$NaO_{0.5}$	0.104	0.221	0.207	0.178	0.102	0.146	0.245	0.275	0.238	0.202
$AlO_{1.5}$	0.059	0.092	0.089	0.083	0.112	0.149	0.225	0.249	0.230	0.210
SiO_2	0.852	1.145	1.183	1.259	1.254	1.449	1.808	2.017	2.264	2.521
Bulk	1.015	1.458	1.479	1.520	1.469	1.744	2.278	2.541	2.732	2.933

Explanation: "Excess" is the difference between observed and predicted values; polymerized and unpolymerized entries are excess and predicted values, except for silica, for which calculated $Si_2O_{4,aq}$ is included in polymerized SiO_2. Observed values at 600 °C, 1 GPa from Manning et al. (2010); predicted values at this P and T differ slightly due to our use of Holland and Powell (1998) mineral data. *Abbreviations:* A, albite; J, jadeite; P, paragonite; Q, quartz.

namic data (Manning et al., 2010). Though we used a different method to bracket the fluid composition at albite–paragonite–quartz or jadeite–paragonite–quartz, we obtain results comparable to Manning et al. (2010) at the same P–T conditions, and the trends in Na/Al in our study agree with those established by previous work (Morey and Hesselgesser, 1951; Currie, 1968; Anderson and Burnham, 1983; Manning et al., 2010). Thus, differences in methodology are not a likely source of the discrepancy.

Inaccuracy in the extrapolated thermodynamic properties is another potential source of the differences between calculated fluid composition and our experimental results. Thermodynamic databases, especially for ions, have many sources of error (e.g., Oelkers et al., 2009). However, several considerations suggest that this is not responsible for the variance. First, the equations for the solubility of quartz (Manning, 1994) and aqueous silica speciation (Newton and Manning, 2002, 2003) are included in the calculations. These are based on experimental determinations at the same conditions of this study. Leaving aside the other components of the solution, the silica concentrations alone should agree well; but they in fact diverge to the greatest degree on an absolute basis. In addition, the extrapolation scheme used to compute equilibrium constants successfully reproduces experimentally derived mineral solubility in H_2O in systems that are compositionally simpler, including corundum solubility in H_2O (e.g., Manning, 2007; Tropper and Manning, 2007) and corundum solubility in KOH–H_2O (Wohlers and Manning, 2009). Finally, Manning et al. (2010) showed that even in this compositionally complex system, the extrapolation scheme reproduces experimentally constrained solubilities at low temperatures of <500 °C at 1 GPa. Thus, errors in thermodynamic data, while they certainly exist, can not alone cause the difference between the calculations and the experiments.

The origin of the solubility excess in experimental fluids is better explained by the presence of solutes that are not taken into account in predicting the fluid compositions. These missing species must be the predominant reservoirs for all three elements over the entire P–T range of this investigation. At 500 °C, Na, Al and Si exceed predicted values by 54%, 64%, and 40% (molar) on average. Similarly, at 600 °C, the mean molar excesses are even greater: Na, 79%; Al, 77%; Si, 58%.

Because the calculation scheme for predicting solubility included all significant monomers, ions, and simple species, the dissolved structures needed to explain the excess solubility must be more polymerized solutes (Manning et al.,

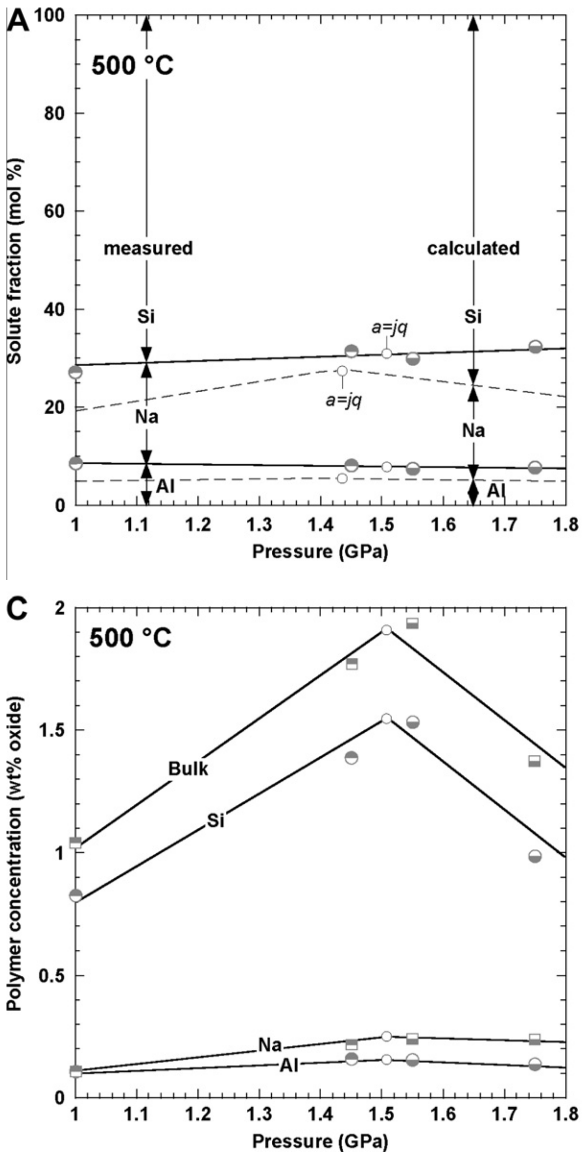

Fig. 6. Elemental solute fractions (A and B) and predicted polymer concentrations (C and D). Experimentally determined element fractions (solid lines, in mol%) at 500 °C (A) and 600 °C (B) differ from predicted values (dashed lines) at all conditions investigated. Measured fluid compositions have higher Al fraction, and lower Si fraction than predicted. The concentrations of the polymerized fraction of each element (in wt% oxide) at 500 °C (C) and 600 °C (D) displays the same pattern as the total solubility (Fig. 6) because these species predominate in the solutions at all conditions studied. Small open circles denote the experimentally constrained or calculated (Holland and Powell, 1998) position of Eq. (1).

2010). This inference is supported by growing spectroscopic and phase equilibrium evidence for the presence of polymeric solute structures at high P and T (e.g., Mysen, 1998; Salvi et al., 1998; Zhang and Frantz, 2000; Zotov and Keppler, 2000, 2002; Newton and Manning, 2002, 2003, 2008; Manning, 2004, 2007; Mibe et al., 2008). The calculations included $NaAlO_{2,aq}$, $NaHSiO_{3,aq}$, and the silica dimer $Si_2O_{4,aq}$, so the additional solutes must involve even more complex stoichiometry and composition, and all elements must participate. In light of the previous studies, the proposed polymeric solutes likely involve a mixture of linear and ring structures, with an abundance that varies with P and T in a manner that accommodates the changing bulk solute concentration and element fractions.

The concentration of the inferred polymerized solutes rises with P in the albite stability field, attains a maximum at the position of Eq. (1), and declines with further P increase in the jadeite stability field (Table 4 and Fig. 6C, D). At the jadeite–albite–quartz equilibrium, the bulk polymerized fraction constitutes nearly 2 wt% (of ~3.3 wt% total dissolved solutes) at 500 °C, and ~7.9 wt% (of ~10.3 wt%) at 600 °C. Polymerized species are dominated by SiO_2 at all conditions investigated, with $NaO_{0.5}$ and $AlO_{1.5}$ present in broadly subequal concentrations (Fig. 6C and D).

4.4. Origin of solubility patterns

The main solubility patterns revealed by our experiments are an isobaric increase in solubility with T, and an isothermal maximum in solubility at the position of Eq. (1). Fig. 7 illustrates that these patterns result in bulk-solubility isopleths with negative dP/dT in the albite stability field, but positive dP/dT in the jadeite stability field. This differs from a predicted pattern of negative dP/dT at all P and T (Fig. 5D). Because the inferred polymeric components are predominant among the solutes, their behavior must govern the solubility patterns (Figs. 5–7). We suggest two primary controls on this behavior.

Based on isobaric experiments at 1 GPa, Manning et al. (2010) proposed that increasing Na–Al–Si polymer solubility is linked to the approach to the hydrothermal melting point, reflecting increasing stability in the fluid of the structural elements that will comprise the melt phase when it becomes stable. Our results are consistent with this hypothesis. As shown in Fig. 7, isobaric sections at P higher than 1 GPa intersect the melting curve in the albite stability field at progressively lower T, owing to the negative Clapeyron slope of the hydrothermal melting curve of albite + quartz. If the hypothesis of premelting stabilization of polymeric solutes is correct, then isobaric approach to melting at progressively higher P should yield greater excess solubility (higher polymer concentration) in the albite field. Our data show that this is the observed solubility pattern. Moreover, in the jadeite stability field, the Clapeyron slope of hydrothermal melting of jadeite + quartz is positive, so isobaric experiment-pairs at 500 and 600 °C grow more distant from the melting point as P increases. If the premelting hypothesis is correct, increasing the P of isobaric sections should yield decreasing solubility excesses (progressively lower polymer concentration). Again, this is the result returned by our data. In short, the experimental results lend support to the hypothesis that there is a strong increase in polymerization of Na–Al–Si solutes within ~100–150 °C of hydrothermal melting point in this system.

The slopes of the solubility isopleths and the hydrothermal melting curves exhibit a change in sign when the albite = jadeite + quartz equilibrium is encountered. These changes in sign arise from the large difference between the molar volumes of albite and jadeite. Neither melt nor aqueous solutes will exhibit a first-order-like volume change; rather, their changes on isothermal compression will be continuous and small. Thus, the volume change of the solids dictates the topology of the isopleths, as it does the hydrothermal melting curve.

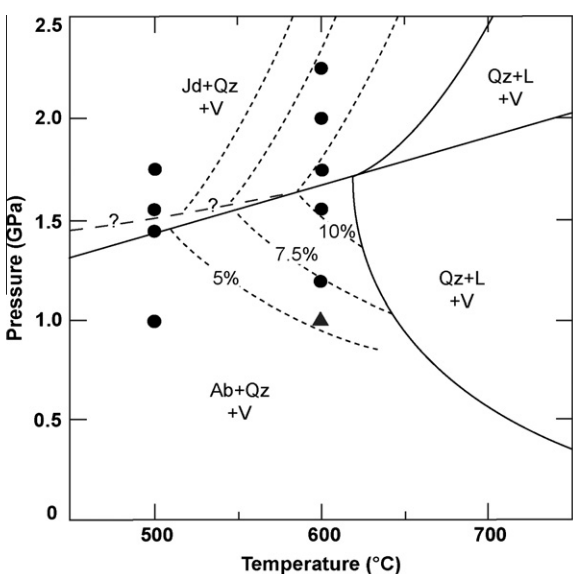

Fig. 7. P–T diagram showing conditions of experiments (filled circles, this study; triangle, Manning et al., 2010) and bulk solubility isopleths (short dashed lines) in wt% oxides. Paragonite present below solidus but supersolidus phase relations uncertain. Solid lines show position of Eq. (1) (Holland and Powell, 1998) and hydrothermal melting of albite + quartz and jadeite + quartz. Queried long-dashed line shows position of Eq. (1) consistent with 500 °C experiments in the present study. Hydrothermal melting curves after Luth et al. (1964; adjusted by Luth, 1968), Boettcher and Wyllie (1969) and Manning et al. (2010). It was assumed for simplicity that there are no critical end points on the melting curves; this is broadly consistent with the experimental studies, but none report sufficiently tight reversals near Eq. (1) to assess potential critical behavior in the system. There are insufficient data to accurately portray the topologies of the critical mixing curves for liquid + vapor in either the albite + quartz or jadeite + quartz fields.

4.5. Implications for metamorphic fluids

Several insights into high-P metasomatic fluids arise from this work. First, the crossing of reaction boundaries during burial and exhumation may trigger abrupt changes in solubility patterns, with potentially important implications for mass transfer. As shown in Figs. 6 and 7, the maximum solubility at a given T is encountered at the albite = jadeite + quartz boundary. A fluid rising nearly isothermally from the jadeite stability field will dissolve rock constituents along its path until encountering Eq. (1). With further decompression, solubilities instead decline, forcing mineral precipitation to maintain equilibrium. Thus, the reaction boundary represents a transition from mineral dissolution to mineral precipitation. With the caveat that this is a very simple chemical system, the changes highlight how flow of metamorphic fluid can participate in large-scale chemical transfers and crustal evolution.

Our study supports the hypothesis that metamorphic systems may experience enhanced metasomatism as they approach melting conditions (Manning et al., 2010). Fluid movement through, or loss from, a given volume of metamorphic rock near its melting point can lead to significant bulk compositional change because of the very high solubilities in this P–T region. This could complicate interpretation of leucosome–melanosome compositional relations if the rocks eventually melt and form migmatites.

The new experiments have particular relevance to metasomatic mass transfer in subduction zones. Some model P–T paths of slab tops display a strong T increase from <400 to >600 °C at 2.0 ± 0.5 GPa, corresponding to the onset of coupling between the slab and mantle wedge (e.g., Syracuse et al., 2010). Extrapolating from our model chemical system, it can be concluded that fluids which equilibrate with the uppermost metabasalts and sediments at these conditions prior to exit into the mantle wedge will carry a large solute load, chiefly in the form of polymeric complexes. These solution components have the capacity to metasomatize the mantle wedge, both in consequence of their essential structural elements (alkalis, Al, and Si), as well as by providing structural environments that readily incorporate trace refractory constituents (e.g., Manning, 2004; Manning et al., 2008).

5. CONCLUSIONS

(1) Albite + quartz and jadeite + quartz dissolve incongruently in H_2O over the investigated P–T range, leaving the aluminum-rich residual phase paragonite.
(2) In the albite stability field, the solubilities of all elements (and accordingly, bulk solubility), rise with isothermal P increase, to a maximum at the albite = jadeite + quartz equilibrium. In the jadeite stability field, all element solubilities decline with further isothermal P increase. At a given P, all element solubilities are higher at 600 °C than at 500 °C. The solubility of Si is greater than Na or Al. Silica solubilities exceed those measured in H_2O equilibrated with albite or quartz alone. All measured fluid compositions are peralkaline (Na/Al > 1). Molar Na/Al rises with P at constant T, but decreases with T at constant P.
(3) Element and bulk solubilities in measured fluids are higher than predicted at all P and T investigated. Because the model fluids only account for simple monomeric species and ions, and the silica dimer, the excess solubility signals the presence of polymerized species in the solutions. These species must accommodate all three elements, and are likely a mix of a variety of structures in varying ratios and stoichiometries. They are the predominant solutes in solution.
(4) The solubility patterns are best explained by a model in which polymerization of solutes proceed as the melting point is approached. The solubility maximum at the albite = jadeite + quartz equilibrium translates to a change in the sign of dP/dT of solubility isopleths. Like the change in sign of the Clapeyron slope of the hydrothermal melting curves, this behavior owes its origin to the large volume difference between albite and jadeite.
(5) The new solubility data have important consequences for metamorphic fluids. They show that reaction boundaries with large ΔV can drive mineral precipitation from buoyantly rising fluids. Moreover, metamorphic systems may experience dramatic bulk compositional change prior to melting, owing to the enhanced metasomatic power of near-solidus fluids. This could complicate interpretation of compositional relations in rocks that eventually melted, such as migmatites. Finally, fluids leaving subducting slabs will carry very high solute loads, mainly in the form of polymerized species. These species could effectuate important mass transfer of otherwise insoluble materials.

ACKNOWLEDGMENTS

This work was supported by the ETH Zurich and the National Science Foundation Grant EAR-0711521 to C.E.M. We thank R. Newton for discussions and assistance. Reviews and comments by E. Oelkers, A. Liebscher, G. Anderson and an anonymous reviewer improved the manuscript.

APPENDIX

At a given P and T in the albite stability field, heterogeneous equilibrium can be described by:

$$\underset{\text{albite}}{3\mathrm{NaAlSi_3O_8}} + 2\mathrm{H^+} = \underset{\text{paragonite}}{\mathrm{NaAl_3Si_3O_{10}(OH)_2}} + \underset{\text{quartz}}{6\mathrm{SiO_2}} + 2\mathrm{Na^+} \tag{A1}$$

and

$$\underset{\text{albite}}{\mathrm{NaAlSi_3O_8}} + 2\mathrm{AlO_2^-} + 2\mathrm{H^+} = \underset{\text{paragonite}}{\mathrm{NaAl_3Si_3O_{10}(OH)_2}} \tag{A2}$$

In the jadeite stability field, the corresponding equilibria are

$$\underset{\text{jadeite}}{3\mathrm{NaAlSi_2O_6}} + 2\mathrm{H^+} = \underset{\text{paragonite}}{\mathrm{NaAl_3Si_3O_{10}(OH)_2}} + \underset{\text{quartz}}{3\mathrm{SiO_2}} + 2\mathrm{Na^+} \tag{A3}$$

and

$$\underset{\text{jadeite}}{\mathrm{NaAlSi_2O_6}} + \underset{\text{quartz}}{\mathrm{SiO_2}} + 2\mathrm{AlO_2^-} + 2\mathrm{H^+} = \underset{\text{paragonite}}{\mathrm{NaAl_3Si_3O_{10}(OH)_2}} \tag{A4}$$

An additional eight equilibria are independent of albite or jadeite stability:

$$\mathrm{H_2O} = \mathrm{H^+} + \mathrm{OH^-} \tag{A5}$$

$$\underset{\text{quartz}}{\mathrm{SiO_2}} + \mathrm{H_2O} = \mathrm{HSiO_3^-} + \mathrm{H^+} \tag{A6}$$

$$\mathrm{HAlO_{2,aq}} = \mathrm{H^+} + \mathrm{AlO_2^-} \tag{A7}$$

$$\mathrm{NaOH_{aq}} = \mathrm{Na^+} + \mathrm{OH^-} \tag{A8}$$

$$\mathrm{NaAlO_{2,aq}} = \mathrm{Na^+} + \mathrm{AlO_2^-} \tag{A9}$$

$$\underset{\text{quartz}}{\mathrm{SiO_2}} + \mathrm{NaOH_{aq}} = \mathrm{NaHSiO_{3,aq}} \tag{A10}$$

$$\underset{\text{quartz}}{\mathrm{SiO_2}} = \mathrm{SiO_{2,aq}} \tag{A11}$$

$$2\mathrm{SiO_{2,aq}} = \mathrm{Si_2O_{4,aq}} \tag{A12}$$

The activities of the charged aqueous species can be derived from equations for the equilibrium constants (K) for Eqs. (A1)–(A6). By adopting standard states for pure minerals and H_2O of unit activity of the pure phase at any P and T, four constraints are provided by the mass-action expressions for Eqs. (A1)–(A6):

$$K_5 = a_{\mathrm{H^+}} a_{\mathrm{OH^-}} \tag{A13}$$

$$K_6 = a_{\mathrm{HSiO_3^-}} a_{\mathrm{H^+}} \tag{A14}$$

and, in the albite stability field,

$$K_1 = \left(\frac{a_{Na^+}}{a_{H^+}}\right)^2 \tag{A15}$$

$$K_2 = (a_{AlO_2^-} a_{H^+})^{-2} \tag{A16}$$

or, in the jadeite stability field,

$$K_3 = \left(\frac{a_{Na^+}}{a_{H^+}}\right)^2 \tag{A17}$$

$$K_4 = (a_{AlO_2^-}\ a_{H^+})^{-2} \tag{A18}$$

where a is the activity of the subscripted species or phase. The final constraint is provided by the charge balance requirement:

$$m_{H^+} + m_{Na^+} - m_{OH^-} - m_{AlO_2^-} - m_{HSiO_3^-} = 0 \tag{A19}$$

Species concentrations may be substituted for activities in Eqs. (A13)–(A18) using $a_i = \gamma_i m_i$, where γ_i is activity coefficient of the subscripted species, by using a standard state for aqueous species of unit activity of the hypothetical 1 m solution. Ion activity coefficients were calculated from the Güntelberg equation:

$$\mathrm{Log}\,\gamma_i = -\frac{Az_i^2\sqrt{I}}{1+\sqrt{I}} \tag{A20}$$

where z is ion charge, I is ionic strength, and A is the solvent parameter, here assumed to be unity following arguments of Manning (1998, 2007). The Güntelberg equation was used because of its simplicity and has been proven accurate in independent studies at these conditions (Manning, 2007; Wohlers and Manning, 2009). Because our analysis involves only monovalent ions, $\gamma_i = \gamma_1$, and Eq. (A20) simplifies to $\log\gamma_1 = -\sqrt{I}/(1+\sqrt{I})$. This leads to the following expressions for charged species concentrations in the albite stability field:

$$m_{H^+} = \frac{1}{\gamma_1}\left(\frac{K_5 + K_2^{-1/2} + K_6}{K_1^{1/2}+1}\right) \tag{A21}$$

$$m_{OH^-} = \frac{K_5}{\gamma_1^2 m_{H^+}} \tag{A22}$$

$$m_{AlO_2^-} = \frac{1}{\gamma_1^2 m_{H^+} K_2^{1/2}} \tag{A23}$$

$$m_{Na^+} = K_1^{1/2} m_{H^+} \tag{A24}$$

$$m_{HSiO_3^-} = \frac{K_6}{\gamma_1^2 m_{H^+}} \tag{A25}$$

Charged species concentrations in the jadeite stability field are derived by substituting K_3 for K_1 and K_4 for K_2 in the above equations. The concentrations of neutral species follow from these equations and the assumption of unit activity coefficients (Walther and Helgeson, 1977; Manning, 1998, 2007; Newton and Manning, 2003, 2008; Wohlers and Manning, 2009):

$$m_{HAlO_{2,aq}} = \frac{\gamma_1^2 m_{H^+} m_{AlO_2^-}}{K_7} \tag{A26}$$

$$m_{NaOH_{aq}} = \frac{\gamma_1^2 m_{Na^+} m_{OH^-}}{K_8} \tag{A27}$$

$$m_{NaAlO_{2,aq}} = \frac{\gamma_1^2 m_{Na^+} m_{AlO_2^-}}{K_9} \tag{A28}$$

$$m_{NaHSiO_{3,aq}} = m_{NaOH_{aq}} K_{10} \tag{A29}$$

$$m_{SiO_{2,aq}} = K_{11} \tag{A30}$$

$$m_{Si_2O_{4,aq}} = m_{SiO_{2,aq}} K_{12} \tag{A31}$$

Derivation of equilibrium constants for Eqs. (A1)–(A10) follows methods described by Manning (1998, 2007), Wohlers and Manning (2009), and Manning et al. (2010). Equilibrium constants were calculated in increments of 50 MPa from 0.3 to 0.5 GPa using thermodynamic data of Holland and Powell (1998; 2002 update) for minerals and Pokrovskii and Helgeson (1997) for aqueous species. We used the Haar et al. (1984) equation of state of H_2O to ensure consistency with the thermodynamic properties of aqueous species derived within this framework. As illustrated in Fig. A1, all log Ks vary linearly with the logarithm of H_2O density. Accordingly, log K values at experimental conditions were obtained by linear extrapolation from 0.3 to 0.5 GPa (Table 3 and Fig. A1). Values for log K_5 and log K_6 derived this way imply incorrect P of Eq. (1). We found that, in detail, the trends in these log K values with log ρ_{H_2O} were slightly nonlinear. We therefore adopted an alternative approach in which internal consistency was insured by obtaining log K_3 and log K_4 from extrapolated log K_1 and log K_2 via

$$\mathrm{Log}\,K_3 = \log K_1 - 3\log K_{ajq} \tag{A32}$$

$$\mathrm{Log}\,K_4 = \log K_{ajq} - \log K_2 \tag{A33}$$

where K_{ajq} is the equilibrium constants for Eq. (1), text. Equilibrium constants for Eqs. (A11) and (A12) were derived from the standard Gibbs free energy of quartz

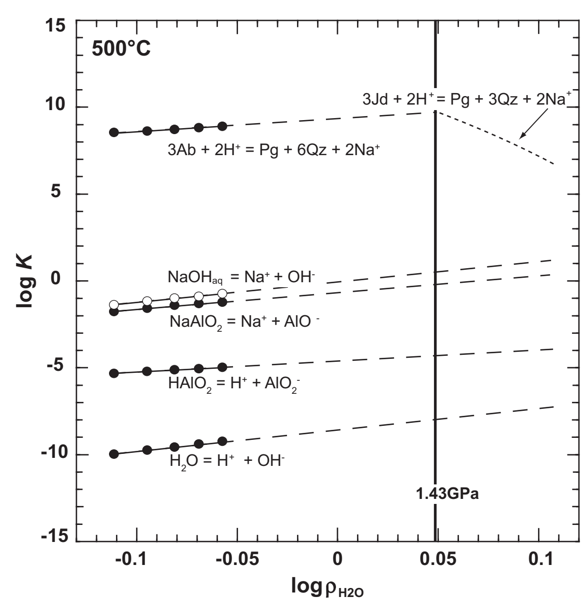

Fig. A1. Variation in log K with log ρ_{H_2O} at 500 °C for representative equilibria (see text). Symbols represent calculated log K from 0.3 to 0.5 GPa, at 0.05 GPa increments. The log K values vary linearly with log ρH_2O (cf. Manning, 1998, 2007). Dashed lines show linear extrapolations to 2.25 GPa; the dash-dot line represents log K_1 − 3log K_{ajq} (see text).

(Holland and Powell, 1998; 2002 update), quartz solubility from Manning (1994), and the silica speciation model of Newton and Manning (2002, 2003). It was assumed that the pressure dependence of the monomer-dimer reaction (Eq. (A12)), determined at 700 °C by Newton and Manning (2002), is independent of temperature.

REFERENCES

Anderson G. M. and Burnham C. W. (1965) The solubility of quartz in supercritical water. *Am. J. Sci.* **263**, 494–511.

Anderson G. M. and Burnham C. W. (1983) Feldspar solubility and the transport of aluminum under metamorphic conditions. *Am. J. Sci.* **283**, 283–297.

Ague J. J. (1994a) Mass-transfer during Barrovian metamorphism of pelites, south-central Connecticut: 1. Evidence for changes in composition and volume. *Am. J. Sci.* **294**, 989–1057.

Ague J. J. (1994b) Mass-transfer during Barrovian metamorphism of pelites, south-central Connecticut: 2. Channelized fluid-flow and the growth of staurolite and kyanite. *Am. J. Sci.* **294**, 1061–1134.

Ague J. J. (1995) Deep-crustal growth of quartz, kyanite and garnet into large-aperture, fluid-filled fractures, north-eastern Connecticut, USA. *J. Metamorph. Geol.* **13**, 299–314.

Ague J. J. (1997) Crustal mass transfer and index mineral growth in Barrow's garnet zone, northeast Scotland. *Geology* **25**, 73–76.

Ague J. J. (2003) Fluid infiltration and transport of major, minor, and trace elements during regional metamorphism of carbonate rocks, Wepawaug Schist, Connecticut, USA. *Am. J. Sci.* **303**, 753–816.

Antignano A. and Manning C. E. (2008) Rutile solubility in H_2O, H_2O–SiO_2 and H_2O–$NaAlSi_3O_8$ at 0.7–2.0 GPa and 700–1000 °C: implications for mobility of nominally insoluble elements in geologic fluids. *Chem. Geol.* **255**, 283–293.

Ayers J. C. and Watson E. B. (1991) Solubility of apatite, monazite, zircon, and rutile in supercritical aqueous fluids with implications for subduction zone geochemistry. *Philos. Trans. R. Soc. Lond. A* **335**, 365–375.

Boettcher A. L. and Wyllie P. J. (1969) Phase relationships in the system $NaAlSiO_4$–SiO_2–H_2O to 35 kilobars pressure. *Am. J. Sci.* **267**, 875–909.

Chatterjee N. D. (1972) The upper stability limit of the assemblage paragonite + quartz and its natural occurrences. *Contrib. Mineral. Petrol.* **34**, 288–303.

Coleman R. G. (1961) Jadeite deposits of the Clear Creek area, New Idria District, San Benito County, California. *J. Petrol.* **2**, 209–247.

Currie K. L. (1968) On the solubility of albite in supercritical water in the range 400 to 600 °C and 750 to 3500 bars. *Am. J. Sci.* **266**, 321–341.

Fockenberg T., Burchard M. and Maresch W. V. (2006) Experimental determination of the solubility of natural wollastonite in pure water up to pressures of 5 GPa and at temperatures of 400–800 °C. *Geochim. Cosmochim. Acta* **70**, 1796–1806.

Fockenberg T., Burchard M. and Maresch W. V. (2008) The solubility of natural grossular-rich garnet in pure water at high pressures and temperatures. *Eur. J. Mineral.* **20**, 845–855.

Haar L., Gallagher J. S. and Kell G. S. (1984) NBSINRC steam Tables. *Hemisphere, New York, P.*, 320.

Hays J. F. and Bell P. M. (1973) Albite–jadeite–quartz equilibrium: a hydrostatic determination. *Carnegie Inst. Wash. Yearbook* **72**, 706–708.

Hemley J. J., Meyer C. and Richter D. H. (1961) Some alteration reactions in the system Na_2O–Al_2O_3–SiO_2–H_2O. U.S. Geol. Survey Professional Paper 434D, pp. 338–340.

Holland T. J. B. (1980) The reaction albite = jadeite + quartz determined experimentally in the range 600–1200 °C. *Am. Mineral.* **65**, 129–134.

Holland T. J. B. and Powell R. (1998) An internally consistent thermodynamic data set for phases of petrological interest. *J. Metamorph. Geol.* **16**, 309–343.

Luth W. C. (1968) The influence of pressure on the composition of eutectic liquids in the binary systems sanidine silica and albite–silica. *Carnegie Inst. Wash. Yearbook* **66**, 480–484.

Luth W. C., Jahns R. H. and Tuttle O. F. (1964) The granite system at pressures of 4 to 10 kilobars. *J. Geophys. Res.* **69**, 759–773.

Manning C. E. (1994) The solubility of quartz in H_2O in the lower crust and upper mantle. *Geochim. Cosmochim. Acta* **58**, 4831–4839.

Manning C. E. (1998) Fluid composition at the blueschist–eclogite transition in the model system Na_2O–Al_2O_3–SiO_2–H_2O–HCl. *Schweiz. Mineral. Petrogr. Mitt.* **78**, 225–242.

Manning C. E. (2004) The chemistry of subduction-zone fluids. *Earth Planet. Sci. Lett.* **223**, 1–16.

Manning C. E. (2007) Solubility of corundum + kyanite in H_2O at 700 °C and 10 kbar: evidence for Al–Si complexing at high pressure and temperature. *Geofluids* **7**, 258–269.

Manning C. E. and Boettcher S. L. (1994) Rapid-quench hydrothermal experiments at mantle pressures and temperatures. *Am. Mineral.* **79**, 1153–1158.

Manning C. E., Wilke M., Schmidt C. and Cauzid J. (2008) Rutile solubility in albite-H_2O and $Na_2Si_3O_7$-H_2O at high temperatures and pressures by in-situ synchrotron radiation micro-XRF. *Earth Planet. Sci. Lett.* **272**, 730–737.

Manning C. E., Antignano A. and Lin H. A. (2010) Premelting polymerization of crustal and mantel fluids, as indicated by the solubility of albite + paragonite + quartz in H2O at 1 GPa and 350–620 °C. *Earth Planet. Sci. Lett.* **292**, 325–336.

Mibe K., Chou I. M. and Bassett W. A. (2008) In situ Raman spectroscopic investigation of the structure of subduction-zone fluids. *J. Geophys. Res.* **113**, 1–8.

Morey G. W. and Hesselgesser J. M. (1951) The solubility of some minerals in superheated steam at high pressures. *Econ. Geol.* **46**, 821–835.

Morey G. W. and Chen W. T. (1955) The action of hot water on some feldspars. *Am. Mineral.* **40**, 996–1000.

Mysen B. O. (1998) Interaction between aqueous fluid and silicate melt in the pressure and temperature regime of the Earth's crust and upper mantle. *Neues Jahrb. Mineral. Abh.* **172**, 227–244.

Newton R. C. and Manning C. E. (2002) Solubility of enstatite + forsterite in H_2O at deep crust/upper mantle conditions: 4 to 15 kbar and 700 to 900 °C. *Geochim. Cosmochim. Acta* **66**, 4165–4176.

Newton R. C. and Manning C. E. (2003) Activity coefficient and polymerization of aqueous silica at 800 °C, 12 kbar, from solubility measurements on SiO_2-buffering mineral assemblages. *Contrib. Mineral. Petrol.* **146**, 135–143.

Newton R. C. and Manning C. E. (2006) Solubilities of corundum, wollastonite and quartz in H_2O–NaCl solutions at 800 °C and 10 kbar: interaction of simple minerals with brines at high pressure and temperature. *Geochim. Cosmochim. Acta* **70**, 5571–5582.

Newton R. C. and Manning C. E. (2007) Solubility of grossular, $Ca_3Al_2Si_3O_{12}$, in H_2O–NaCl solutions at 800 °C and 10 kbar, and the stability of garnet in the system $CaSiO_3$–Al_2O_3–H_2O–NaCl. *Geochim. Cosmochim. Acta* **71**, 5191–5202.

Newton R. C. and Manning C. E. (2008) Thermodynamics of SiO_2–H_2O fluid near the upper critical end point from quartz solubility measurements at 10 kbar. *Earth Planet. Sci. Lett.* **274**, 241–249.

Newton R. C., Manning C. E., Hanchar J. M. and Finch R. J. (2005) Free energy of formation of zircon from aqueous solubility measurements at high temperature and pressure. *J. Am. Ceram. Soc.* **88**, 1854–1858.

Newton R. C., Manning C. E., Hanchar J. M. and Colasanti C. V. (2010) Free energy of formation of zircon based on solubility measurements at high temperature and pressure. *Am. Mineral.* **95**, 52–58.

Oelkers R. H., Bénézeth P. and Pokrovski G. S. (2009) Thermodynamic databases for water–rock interaction. *Rev. Mineral. Geochem.* **70**, 1–46.

Pokrovskii V. A. and Helgeson H. C. (1997) Thermodynamic properties of aqueous species and solubilities of minerals at high pressure and temperatures: the system Al_2O_3–H_2O–KOH. *Chem. Geol.* **137**, 221–242.

Ryabchikov I. D. and MacKenzie W. S. (1985) Interaction of jadeite with water at 20–30 kbar and 650 °C. *Mineral. Mag.* **49**, 601–603.

Ryabchikov I. D. and Boettcher A. L. (1980) Experimental evidence at high pressure for potassic metasomatism in the mantle of the Earth. *Am. Mineral.* **65**, 915–919.

Ryabchikov I. D., Schreyer W. and Abraham K. (1982) Compositions of aqueous fluids in equilibrium with pyroxenes and olivines at mantle pressures and temperatures. *Contrib. Mineral. Petrol.* **79**, 80–84.

Salvi S., Pokrovski G. S. and Schott J. S. (1998) Experimental investigation of aluminum–silica aqueous complexing at 300 °C. *Chem. Geol.* **151**, 51–67.

Schneider M. E. and Eggler D. H. (1986) Fluids in equilibrium with peridotite minerals: implications for mantle metasomatism. *Geochim. Cosmochim. Acta* **50**, 711–724.

Shock E. L., Sassani D. C., Willis M. and Sverjensky D. A. (1997) Inorganic species in geologic fluids: correlations among standard molal thermodynamic properties of aqueous ions and hydroxide complexes. *Geochim. Cosmochim. Acta* **61**, 907–950.

Shmulovich K., Graham C. and Yardley B. (2001) Quartz, albite and diopside solubilities in H_2O–NaCl and H_2O–CO_2 fluids at 0.5–0.9 GPa. *Contrib. Mineral. Petrol.* **141**, 95–108.

Stalder R., Ulmer P., Thompson A. B. and Guenther D. (2000) Experimental approach to constrain second critical end points in fluid/silicate systems: near-solidus fluids and melts in the system albite–H_2O. *Am. Mineral.* **85**, 68–77.

Sverjensky D. A., Shock E. L. and Helgeson H. C. (1997) Prediction of the thermodynamic properties of aqueous metal complexes to 1000 °C and 5 kb. *Geochim. Cosmochim. Acta* **61**, 1359–1412.

Syracuse E. M., van Keken P. E. and Abers G. A. (2010) The global range of subduction zone thermal models. *Phys. Earth Planet. Int.* **183**, 73–90.

Tropper P. and Manning C. E. (2007) The solubility of corundum in H_2O at high pressure and temperature and its implications for Al mobility in the deep crust and upper mantle. *Chem. Geol.* **240**, 54–60.

Walther J. V. and Helgeson H. C. (1977) Calculation of the thermodynamic properties of aqueous silica and the solubility of quartz and its polymorphs at high pressures and temperatures. *Am. J. Sci.* **277**, 1315–1351.

Wang H. M., Henderson G. S. and Brenan J. M. (2004) Measuring quartz solubility by in situ weight-loss determination using a hydrothermal diamond anvil cell. *Geochim. Cosmochim. Acta* **68**, 5197–5204.

Wohlers A. and Manning C. E. (2009) Solubility of corundum in aqueous KOH solutions at 700 °C and 1 GPa. *Chem. Geol.* **262**, 326–333.

Woodland A. B. and Walther J. V. (1987) Experimental determination of the solubility of the assemblage paragonite, albite, and quartz in supercritical H_2O. *Geochim. Cosmochim. Acta* **51**, 365–372.

Zhang Y. G. and Frantz J. D. (2000) Enstatite–forsterite–water equilibria at elevated temperatures and pressures. *Am. Mineral.* **85**, 918–925.

Zotov N. and Keppler H. (2000) In-situ Raman spectra of dissolved silica species in aqueous fluids to 900 °C and 14 kbar. *Am. Mineral.* **85**, 600–604.

Zotov N. and Keppler H. (2002) Silica speciation in aqueous fluids at high pressures and temperatures. *Chem. Geol.* **184**, 71–82.

Associate editor: Eric H. Oelkers